Korea-Australia Rheology Journal
Vol. 18, No. 3, September 2006 pp. 161-167

Numerical analysis of viscoelastic flows in a channel obstructed by an asymmetric array of obstacles

Youngdon Kwon*
Department of Textile Engineering, Sungkyunkwan University, Suwon, Kyunggi-do 440-746, Korea
(Received August 22, 2006; final revision received August 31, 2006)

Abstract

This study presents results on the numerical simulation of Newtonian and non-Newtonian flow in a channel obstructed by an asymmetric array of obstacles for clarifying the descriptive ability of current non-Newtonian constitutive equations. Jones and Walters (1989) have performed the corresponding experiment that clearly demonstrates the characteristic difference among the flow patterns of the various liquids. In order to appropriately account for flow properties, the Navier-Stokes, the Carreau viscous and the Leonov equations are employed for Newtonian, shear thinning and extension hardening liquids, respectively. Making use of the tensor-logarithmic formulation of the Leonov model in the computational scheme, we have obtained stable solutions up to relatively high Deborah numbers. The peculiar characteristics of the non-Newtonian liquids such as shear thinning and extension hardening seem to be properly illustrated by the flow modeling. In our opinion, the results show the possibility of current constitutive modeling to appropriately describe non-Newtonian flow phenomena at least qualitatively, even though the model parameters specified for the current computation do not precisely represent material characteristics.

Keywords : shear thinning, extension thickening, flow over obstacles, Carreau model, Leonov model

1. Introduction

Viscoelastic liquids demonstrate various peculiar flow behaviors, most of which result from nonlinear characteristics of the liquids such as shear thinning and extensional hardening. The work by Jones and Walters (1989) clearly illustrates difference in flow phenomena of viscous and viscoelastic fluids. This paper makes an attempt to answer the question if current numerical modeling can appropriately describe these nonlinear viscoelasticity at least qualitatively.

Distinct non-Newtonian flow behavior occurs almost always at high Deborah number or at high flow rate. Thus in order to analyze it, one has to perform successful numerical modeling of this high Deborah number flow, which has been a formidable task in the field of computational viscoelastic fluid dynamics. Its difficulty may be expressed via lack of proper mesh convergence, solution inaccuracy and violation of positive definiteness of the conformation tensor (violation of strong ellipticity of partial differential equations), which ultimately result in degradation of the whole numerical scheme. Here again we employ in the finite element formulation the tensor-logarithmic transform, which has been first suggested by Fattal and Kupferman (2004) and has also been applied in our previous works (Kwon, 2004; Yoon and Kwon, 2005). It forbids the violation of positive definiteness of the conformation tensor and therefore removes one probable pathological behavior of governing equations.

The first finite element implementation of this new formalism has been performed by Hulsen (2004) and Hulsen and coworkers (2005), who have demonstrated dramatic stabilization of the numerical procedure with the Giesekus constitutive equation. Kwon (2004) and Yoon and Kwon (2005) have given numerical results of the flow modeling in the domain with sharp corners. In comparison with the conventional method, stable computation has been demonstrated even in this flow domain with sharp corners. In the papers, it has been concluded that this new method may work only for constitutive equations proven globally stable.

In this work, we consider the viscoelastic flows in a channel obstructed by an asymmetric array of cylindrical obstacles, which have been experimentally investigated by Jones and Walters (1989). The results explicitly illustrate the qualitative difference of flow behaviors among Newtonian, shear thinning and extension thickening fluids. By qualitative comparison of the numerical results with the experiments, we test some popular non-Newtonian constitutive equations and verify the possibility that they can properly describe these phenomena at least qualitatively.

*Corresponding author: kwon@skku.edu
© 2006 by The Korean Society of Rheology

2. Equations in 2D planar flow

In order to analyze flow behavior of various incompressible fluids, one first requires the equation of motion and continuity equation

$$\rho\left(\frac{\partial \mathbf{v}}{\partial t}+\mathbf{v}\cdot\nabla\mathbf{v}\right)=-\nabla p+\nabla\cdot\boldsymbol{\tau},\quad \nabla\cdot\mathbf{v}=0. \tag{1}$$

Here ρ is the density of the liquid, $\mathbf{v}$ the velocity, $\boldsymbol{\tau}$ the extra-stress tensor, and p is the pressure. The gravity force is neglected in the analysis and ∇ is the usual gradient operator in tensor calculus. When kinematic description of the extra-stress is given in terms of the specific constitutive model, the set of governing equations becomes complete.

This study considers three types of fluids such as Newtonian, shear-thinning viscous and viscoelastic liquids. First for Newtonian and shear-thinning liquids the stress tensor is written as

$$\boldsymbol{\tau}=2\eta\mathbf{e}, \tag{2}$$

where $\mathbf{e}=\frac{1}{2}(\nabla\mathbf{v}+\nabla\mathbf{v}^T)$ is the strain rate tensor and η is the viscosity which is constant for the Newtonian liquid. However the viscosity becomes a function of the strain rate for non-Newtonian fluid and thus for suitable expression of the shear-thinning behavior we choose the Carreau model written as

$$\eta=\eta_\infty+(\eta_0-\eta_\infty)[1+(\lambda\dot{\gamma})^2]^{\frac{\mu-1}{2}}. \tag{3}$$

Here η_0 and η_∞ are zero-shear viscosity and asymptotic viscosity at infinite rate of strain, respectively. $\dot{\gamma}=\sqrt{2\mathrm{tr}(\mathbf{e}\cdot\mathbf{e})}$ designates the intensity of the flow and λ and μ are numerical fitting parameters. Thus this viscosity model expresses shear thinning characteristic when $\mu<1$ and $\eta_0>\eta_\infty$.

In expressing viscoelastic property of the liquid, the Leonov constitutive equation (Leonov, 1976) is employed, since it is easy to regulate the degree of extension thickening by proper adjustment of parameters. The differential viscoelastic constitutive equations derived by Leonov can be written into the following quite general form:

$$\boldsymbol{\tau}=(1-s)G\left(\frac{I_1}{3}\right)^n\mathbf{c}+2\eta s\mathbf{e},\quad W=\frac{3G}{2(n+1)}\left[\left(\frac{I_1}{3}\right)^{n+1}-1\right],$$

$$\frac{d\mathbf{c}}{dt}-\nabla\mathbf{v}^T\cdot\mathbf{c}-\mathbf{c}\cdot\nabla\mathbf{v}+\frac{1}{2\theta}\left(\frac{I_1}{I_2}\right)^m\left(\mathbf{c}^2+\frac{I_2-I_1}{3}\mathbf{c}-\boldsymbol{\delta}\right)=\mathbf{0}. \tag{4}$$

Here $\mathbf{c}$ is the elastic Finger strain tensor that describes the accumulated elastic strain in the Finger measure during flow, $\frac{d\mathbf{c}}{dt}=\frac{\partial\mathbf{c}}{\partial t}+\mathbf{v}\cdot\nabla\mathbf{c}$ is the total time derivative of $\mathbf{c}$, $\frac{d\mathbf{c}}{dt}-\nabla\mathbf{v}^T\cdot\mathbf{c}-\mathbf{c}\cdot\nabla\mathbf{v}$ is the upper convected time derivative, G is the modulus, θ is the relaxation time, $\eta=G\theta$ is the total viscosity that corresponds to the zero-shear viscosity and s is the retardation parameter that specifies the solvent viscosity contribution. The tensor $\mathbf{c}$ reduces to the unit tensor $\boldsymbol{\delta}$ in the rest state and this condition also serves as the initial condition in the start-up flow situation. In the asymptotic limit of $\theta\to\infty$ where the material exhibits purely elastic behavior, it becomes the total Finger strain tensor.

$I_1=\mathrm{tr}\,\mathbf{c}$ and $I_2=\mathrm{tr}\,\mathbf{c}^{-1}$ are the basic first and second invariants of $\mathbf{c}$, respectively, and they coincide in planar flows. Due to the characteristic of the Leonov model, the third invariant I_3 satisfies specific incompressibility condition such as $I_3=\det\mathbf{c}=1$. In addition to the linear viscoelastic parameters, it contains 2 nonlinear constants m and n ($n>0$), which can be determined from simple shear and uniaxial extensional flow experiments. They control the strength of shear thinning and extension hardening of the liquid. However the value of the parameter m does not have any effect on the flow characteristics here in 2D situation, since two $\mathbf{c}$ tensor invariants are identical. Thus in this study we adjust only the parameter n to attain appropriate (planar) extension hardening characteristic. The total stress tensor is obtained from the elastic potential W based on the Murnaghan's relation. Since the extra-stress is invariant under the addition of arbitrary isotropic terms, when one presents numerical results it may be preferable to use $\boldsymbol{\tau}=(1-s)G\left(\frac{I_1}{3}\right)^n(\mathbf{c}-\boldsymbol{\delta})+2\eta s\mathbf{e}$ instead in order for the stress to vanish in the rest state.

The essential idea presented by Fattal and Kupferman (2004) in reformulating the constitutive equations is the tensor-logarithmic transformation of $\mathbf{c}$ as follows:

$$\mathbf{h}=\log\mathbf{c}. \tag{5}$$

Here the logarithm operates as the isotropic tensor function, which implies the identical set of principal axes for both $\mathbf{c}$ and $\mathbf{h}$. In the case of the Leonov model, this $\mathbf{h}$ becomes another measure of elastic strain, that is, twice the Hencky elastic strain. While $\mathbf{c}$ becomes $\boldsymbol{\delta}$, $\mathbf{h}$ reduces to $\mathbf{0}$ in the rest state.

In the case of 2D planar flow, the final set of the Leonov constitutive equations in the $\mathbf{h}$-form has been obtained in Kwon (2004) as follows:

$$\frac{\partial h_{11}}{\partial t}+v_1\frac{\partial h_{11}}{\partial x_1}+v_2\frac{\partial h_{11}}{\partial x_2}-\frac{2}{h^2}\left(h_{11}^2+h_{12}^2h\frac{e^h+e^{-h}}{e^h-e^{-h}}\right)\frac{\partial v_1}{\partial x_1}$$
$$-h_{12}\left[\frac{h_{11}}{h^2}\left(1-h\frac{e^h+e^{-h}}{e^h-e^{-h}}\right)+1\right]\frac{\partial v_1}{\partial x_2}$$
$$-h_{12}\left[\frac{h_{11}}{h^2}\left(1-h\frac{e^h+e^{-h}}{e^h-e^{-h}}\right)-1\right]\frac{\partial v_2}{\partial x_1}+\frac{1}{\theta}\frac{e^h-e^{-h}}{2h}h_{11}=0,$$

$$\frac{\partial h_{12}}{\partial t}+v_1\frac{\partial h_{12}}{\partial x_1}+v_2\frac{\partial h_{12}}{\partial x_2}-\frac{2h_{11}h_{12}}{h^2}\left(1-h\frac{e^h+e^{-h}}{e^h-e^{-h}}\right)\frac{\partial v_1}{\partial x_1}$$
$$-\left[\frac{1}{h^2}\left(h_{12}^2+h_{11}^2h\frac{e^h+e^{-h}}{e^h-e^{-h}}\right)-h_{11}\right]\frac{\partial v_1}{\partial x_2}$$

$$-\left[\frac{1}{h^2}\left(h_{12}^2+h_{11}^2 h\frac{e^h+e^{-h}}{e^h-e^{-h}}\right)+h_{11}\right]\frac{\partial v_2}{\partial x_1}$$
$$+\frac{1}{\theta}\frac{e^h-e^{-h}}{2h}h_{12}=0. \quad (6)$$

Here $h=\sqrt{h_{11}^2+h_{12}^2}$ is the eigenvalue of **h**. Actually the total set of eigenvalues in this 2D flow is h, $-h$ and 0. Together with the equations of continuity and motion, Eqs. (6) constitute a complete set to describe isothermal incompressible planar viscoelastic flow. However due to the form presented in Eqs. (6), artificial numerical difficulty may arise. In addition to the case of rest state, during flow vanishing of the eigenvalue h (it means $\mathbf{h}=\mathbf{0}$) may occur locally, *e.g.* along the centerline in the fully developed Poiseuille flow through a straight pipe. Then the coefficients of $\partial v_i/\partial x_j$ and h_{ij} in Eqs. (6) become apparently indeterminate. However proper asymptotic relation for vanishing h can be obtained and given in previous papers (Kwon, 2004; Yoon and Kwon, 2005).

In the notation of the **h** tensor the incompressibility relation $\det \mathbf{c}=1$ becomes

$$\mathrm{tr}\,\mathbf{h}=0. \quad (7)$$

In this 2D analysis, $h_{11}=-h_{22}$, $h_{33}=0$, and thus the viscoelastic constitutive equations add only 2 supplementary unknowns such as h_{11} and h_{12} to the total set of variables.

3. Numerical procedure and boundary conditions

The geometric details of the flow in a channel obstructed by an asymmetric array of cylindrical obstacles are illustrated in Fig. 1. All the arrangement of 4 obstacles coincides with the original experimental setup (Jones and Walters, 1989). Even though employing the periodic boundary condition one can easily solve the flow problem with an infinite number of obstacles, here we consider 4 cylindrical obstacles with traction boundaries at the inlet and outlet.

All the computational scheme except for the boundary conditions is identical with the one employed in the previous studies (Kwon, 2004; Yoon and Kwon, 2005). With the standard Galerkin formulation adopted as basic computational framework, streamline-upwind/Petrov-Galerkin (SUPG) method as well as discrete elastic viscous stress splitting (DEVSS) (Guénette and Fortin, 1995) algorithm is implemented. The upwinding algorithm developed by Gupta (1997) has been applied.

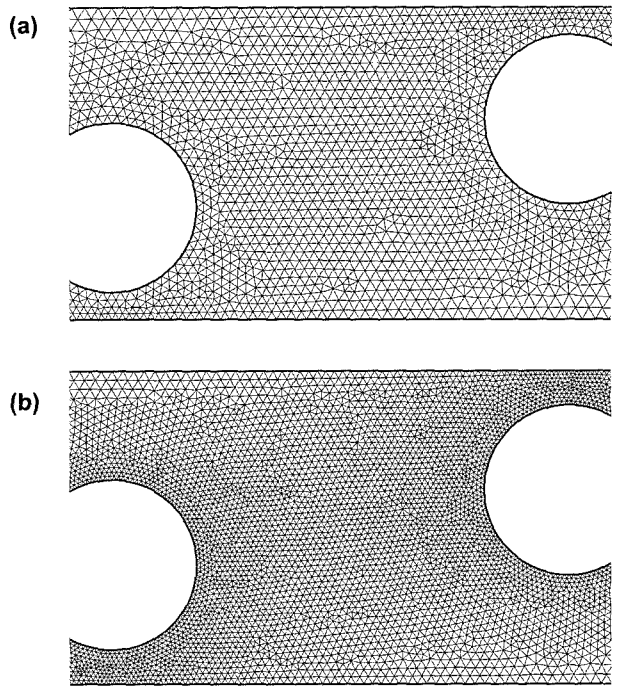

Fig. 2. Partial view of the 2 meshes employed in the computation. (a) coarse mesh, (b) fine mesh.

2 types of meshes are employed and their partial views are illustrated in Fig. 2. Corresponding mesh details are given in Table 1. While the cylindrical obstacle is discretized with 60 straight lines for the coarse mesh, for the finer mesh it is composed of 120 short chords. Even though we have applied 2 types of spatial discretization, the coarse mesh is used only for mesh convergence test and all the theoretical considerations herein are presented on the basis of the results obtained with the finer mesh.

Linear for pressure and strain rate and quadratic interpolations for velocity and **h**-tensor are applied for spatial continuation of the variables. In this work, we only consider steady flow of the isothermal incompressible liquid. In order to mimic dimensionless formulation, we simply

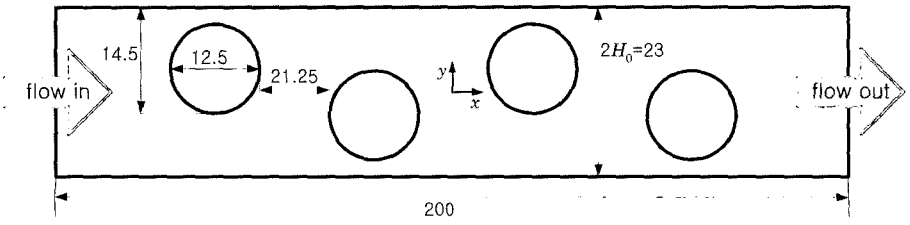

Fig. 1. Schematic diagram of the problem domain for the flow in a channel obstructed by an asymmetric array of cylindrical obstacles.

Table 1. Characteristics of the 2 meshes employed in the computation

	Length of the side of the smallest element	No. of elements	No. of linear nodes	No. of quadratic nodes	No. of unknowns
Coarse mesh	0.5	12786	6748	26285	132132
Fine mesh	0.3	28218	14640	57501	288564

assign unit values for G and θ (Hence the zero-shear viscosity $\eta = G\theta$ also becomes unit) and adjust the Deborah number (or the Reynolds number) by the variation of the average flow rate (actually by varying the traction force at the inlet of the channel). On the other hand, only one set of parameters are employed for the computation of the Carreau viscous model. Their values are $\eta_0 = 1$, $\eta_\infty = 0.1$, $\lambda = 1$ and $\mu = 0.1$.

In order to solve the large nonlinear system of equations introduced, the Newton iteration is used in linearizing the system. As an estimation measure to determine the solution convergence, the L_∞ norm scaled with the maximum value in the computational domain is employed. Hence when the variation of each nodal variable in the Newton iteration does not exceed 10^{-4} of its value in the previous iteration, the algorithm concludes that the converged solution is attained. For the viscoelastic variables, we examine the relative error in terms of the eigenvalue of the **c**-tensor. We have found that this convergence criterion imposes less stringent condition on the computational procedure, and it seems quite practical and appropriate since we mainly observe the results in terms of physically meaningful **c**-tensor or stress rather than **h**.

Here we adopt the traction boundary condition. First all the components of traction vanish at the outlet. On the other hand, in the flow direction (x-axis) at the inlet, the constant finite traction force is applied. In the transverse direction (y-axis), we initially set the boundary free from the traction force. However it is found that in the time-dependent flow computation this boundary condition has introduced some incompatibility, the origin of which is not clear yet. Thus we employ slight modification for the traction in y-direction as follows:

$$t_x = const.,\quad t_y = \frac{t_x}{(L_{channel}/H_0)} \cdot \frac{y}{H_0}, \tag{8}$$

where the total stress tensor $\sigma = -p\delta + \tau$ becomes the traction vector $\boldsymbol{t}$ on the inlet boundary and t_i is its i-th component. $2H_0$ is the height of the channel and $L_{channel}$ is the length of the virtually straight channel, the value of which is specified empirically to guarantee stable computations and set to be $300 \times H_0$ in this computation. This simple modification seems to endow the numerical scheme of transient flow simulation with stability. t_y in Eqs. (8) has been derived from the following estimation of the equation of motion in the flow direction:

$$-\frac{\partial p}{\partial x} + \frac{\partial \tau_{xx}}{\partial x} + \frac{\partial \tau_{xy}}{\partial y} = 0 \;\Rightarrow\; \frac{\partial \tau_{xy}}{\partial y} = -\frac{\partial \sigma_{xx}}{\partial x}$$

$$\Rightarrow \frac{\partial t_y}{\partial y} = -\frac{\partial \sigma_{xx}}{\partial x} \approx const. \approx \frac{t_x}{L_{channel}} \quad \text{on the inlet boundary,}$$

which results in t_y in Eqs. (8).

Certainly one may employ the traction boundary condition obtained from the analytic solution for the fully developed flow along the straight pipe. However it is applicable only for 2D or axisymmetric case, since in the general 3D fully developed flow the analytic solution for the channel with an arbitrary cross-section is not known. Hence in the current flow analysis we implement the simple condition (8) other than the fully developed flow conditions.

4. Results and discussion

This study mainly focuses on the ability of the available constitutive equations for non-Newtonian fluids in describing complex flow phenomena employing computational technique. However before discussing these results, it is worthwhile to mention the accuracy and the stability characteristic of the current numerical scheme augmented by the tensor-logarithmic transformation (5).

Although the detailed result is not presented in this paper, we have found proper characteristics of mesh convergence in the previous works (Kwon, 2004; Yoon and Kwon, 2005) as well as in this study. Since we have adopted not the boundary condition with velocity profile specified but the traction boundaries both at the inlet and outlet, it is probable that the flow rate at the inlet differs from that at the outlet if the incompressibility condition is not appropriately accounted in the computation. However the computational results have shown that the flow rates at the inlet and outlet coincide up to the 13th significant digit.

We define the Deborah number as

$$De = \frac{v_m \theta}{D}, \tag{9}$$

where v_m is the average flow rate at the channel inlet or outlet and $D = 2.5$ is the width of the narrow gap between the cylindrical obstacle and the channel wall. As the Newtonian viscous term becomes relatively large, the stability of the system is dramatically improved. When we specify $s = 0.5$ with $n = 0.1$ and $\rho = 0$ for the Leonov model (4),

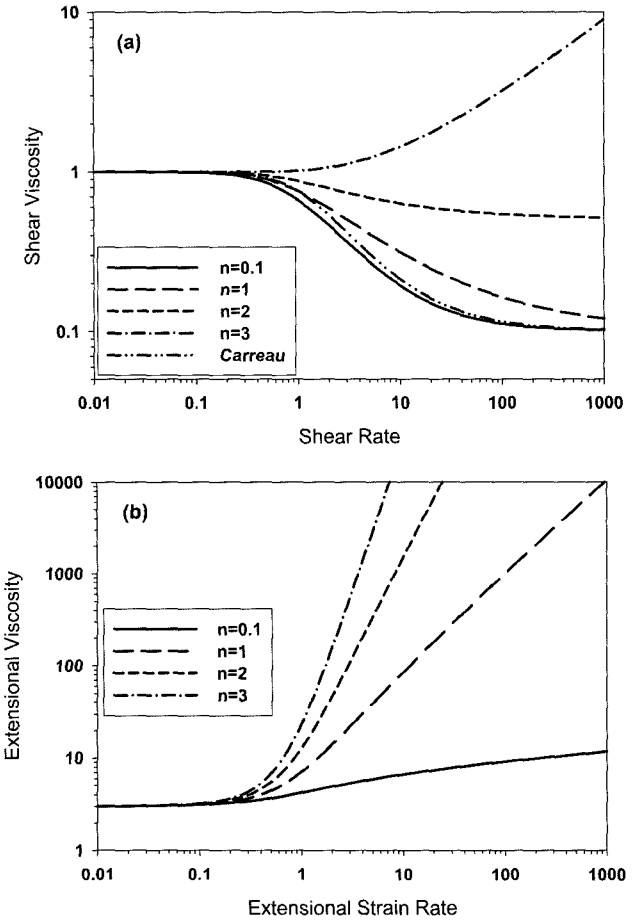

Fig. 3. Steady flow curves for the Leonov model with $s = 0.1$. (a) shear rate vs. shear viscosity in simple shear and (b) extensional strain rate vs. extensional viscosity in uniaxial extension.

we have obtained the stable solution up to $De = 1.2 \times 10^7$ ($t_x/G = 4.7 \times 10^8$) and stopped the computation due to no further interest. This agrees with results obtained in the previous works (Hulsen, 2004; Hulsen *et al.*, 2005). However when s becomes close to 0, the limit Deborah number, over which stable computation cannot be carried out, becomes finite in the range of 4.5~20.

Before we investigate the results, in Fig. 3 the simple flow properties are illustrated. When $n = 0.1$ for the Leonov model, the simple shear flow characteristic is almost identical with that of the Carreau model (Fig. 3a). For $n = 0.1$ and 1, shear thinning behavior is quite distinctly manifested. However in the case of $n = 2$ it is weakly presented and even shear thickening behavior is observed when $n = 3$. Fig. 3(b) depicts extension hardening behavior of the Leonov model for all values of n. The extension hardening moderately appears for $n = 0.1$, while it is strongly expressed when $n > 1$. Here we have controlled the level of extension thickening by the adjustment of n, which also alters the degree of shear thinning. However from the experiments it

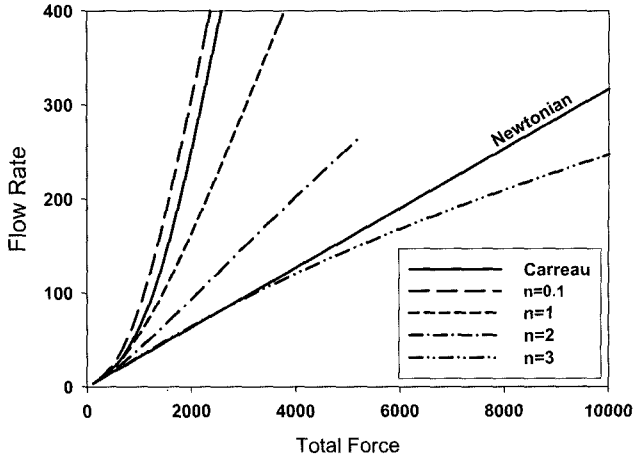

Fig. 4. Total flow rates as functions of the total traction force applied at the inlet boundary for the Newtonian, Carreau and Leonov model fluids ($s = 0.1$, $\rho = 0.001$).

is quite often observed that extension thickening is apparently independent of the shear thinning. For the Leonov model, one may change the extent of uniaxial extensional thickening without varying shear thinning behavior by regulating the value of m in Eqs. (4) with n fixed, but m does not have any effect on the planar extension characteristics which plays an important role in this current 2D flow modeling.

The dependence of the total flow rate in the channel upon the applied force ($t_x \times 2H_0$) at the inlet is shown in Fig. 4 for all types of the liquid. Since the Deborah number cannot be defined for the Newtonian and Carreau viscous liquids, the total flow rate Q is chosen as the output variable. As is expected, the flow rate is monotonically increasing with the traction force for all types. For the Carreau viscous and the Leonov viscoelastic liquids with $n = 0.1$, 1 and 2, the flow rate is higher than that of the Newtonian liquid, which seems to result from their shear thinning behavior. On the other hand the flow rate for the Leonov model with $n = 3$ becomes lower than that of the Newtonian case due to shear thickening as well as severe extension thickening. One can also notice that the flow rate for $n = 0.1$ is somewhat lower than that for the Carreau model, which coincides with its shear thinning viscosity slightly lower than that of the Carreau model.

In Fig. 5, streamlines computed for various liquids are illustrated, where the parameters are chosen to approximately describe the flow behavior depicted in Fig. 25 (figures of the lower Reynolds numbers) of the paper (Jones and Walters, 1989) and to roughly match the Reynolds numbers there. However since we have not determined the model parameters from the basic experimental data, their values do not have rigorous meaning. The arrow in each figure represents relative amount of liquid that goes through wide gaps. In the case of the shear thinning liquid

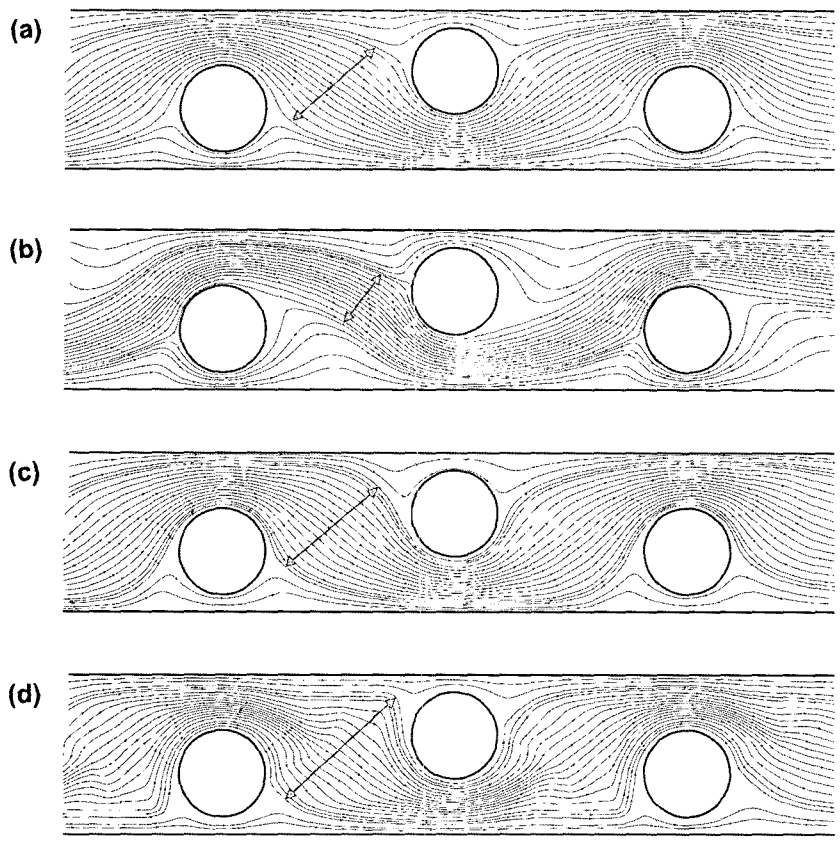

Fig. 5. Streamlines of the flow along the channel obstructed by cylindrical obstacles for (a) Newtonian ($\rho = 0.01$, $Q = 0.1165$), (b) Carreau ($\rho = 0.01$, $Q = 823.8$), (c) viscoelastic ($n = 0.1$, $s = 0.001$, $\rho = 0.01$, $Q = 185.2$) and (d) viscoelastic ($n = 2$, $s = 0.001$, $\rho = 0.01$, $Q = 374.5$) liquids.

(Fig. 5b), the arrow is much shorter than that of the Newtonian liquid and therefore relatively large amount of liquid flows through narrow gaps. This explains significant shear thinning in the flow through the narrow gaps for the Carreau viscous fluid, which results in lowering the viscosity and thus raises the flow rate along the gaps. The extension thickening liquid exhibits quite distinct behavior (Fig. 5d) that the flow rate through the narrow gap becomes low and accordingly the arrow grows longer. This originates from the high extensional viscosity existent in the narrow gap where high extensional flow exists. The flow behavior of the shear thinning viscoelastic liquid (Fig. 5c) is quite similar to that of the Newtonian liquid. In this case we think that both shear thinning and extension hardening compensate for the mutually opposite effects and therefore the appearance of the streamlines becomes analogous to the Newtonian one.

The results of the Newtonian (Fig. 5a), the shear thinning viscous (Fig. 5b) and the extension hardening (Fig. 5d) liquids roughly coincide with those of the Newtonian, the xanthan-gum and polyacrylamide solutions in Fig. 25 of the paper (Jones and Walters, 1989), respectively. In our opinion, in spite of the crude comparison performed in the current study this validates the possibility of current constitutive modeling to appropriately describe non-Newtonian flow phenomena at least qualitatively. For more accurate conclusion, rigorous computational comparison based on experimental verification of model parameters is certainly required.

Fig. 6 presents streamlines for the Carreau viscous fluid

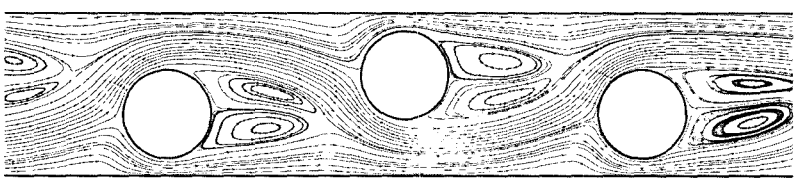

Fig. 6. Streamlines of the flow along the channel obstructed by cylindrical obstacles for Carreau viscous liquid ($\rho = 0.01$, $Q = 2337$).

at higher flow rate that also approximately represent those of the xanthan-gum solution at higher Reynolds number in Fig. 25 of the paper (Jones and Walters, 1989). They demonstrate salient vortices behind the cylinders, which seem to be mainly caused by the inertia force combined with shear thinning.

5. Conclusions

In this study, we have made an attempt to qualitatively describe with available constitutive models complex non-Newtonian phenomena observed in the flow along the channel obstructed by cylindrical obstacles by Jones and Walters (1989). The non-Newtonian response in this flow type is found to be quite distinct from the Newtonian flow behavior in the theoretical as well as experimental aspect. The shear thinning viscous and the extension hardening characteristics exhibited in experiments are quite accurately captured by the computational modeling of the Carreau viscous and the Leonov viscoelastic constitutive equations. In our opinion, in spite of the crude comparison performed in the current study the results show the possibility of current constitutive modeling to appropriately describe non-Newtonian flow phenomena at least qualitatively. For definite estimation of the ability of the constitutive modeling in non-Newtonian fluid mechanics, rigorous computational comparison with model parameters based on experimental verification is certainly essential.

Acknowledgements

This study was supported by research grants from the Korea Science and Engineering Foundation (KOSEF) through the Applied Rheology Center (ARC), an official KOSEF-created engineering research center (ERC) at Korea University, Seoul, Korea.

References

Fattal, R. and R. Kupferman, 2004, Constitutive laws of the matrix-logarithm of the conformation tensor, *J. Non-Newtonian Fluid Mech.* **123**, 281-285.

Guénette, R. and M. Fortin, 1995, A new mixed finite element method for computing viscoelastic flows, *J. Non-Newtonian Fluid Mech.* **60**, 27-52.

Gupta, M., 1997, Viscoelastic modeling of entrance flow using multimode Leonov model, *Int. J. Numer. Meth. Fluids* **24**, 493-517.

Hulsen, M.A., 2004, *Keynote presentation in Internatioan Congress on Rheology 2004*, Seoul, Korea.

Hulsen, M.A., R. Fattal and R. Kupferman, 2005, Flow of viscoelastic fluids past a cylinder at high Weissenberg number: Stabilized simulations using matrix logarithms, *J. Non-Newtonian Fluid Mech.* **127**, 27-39.

Jones, D.M. and K. Walters, 1989, The behavior of polymer solutions in extension-dominated flows, *Rheol. Acta* **28**, 482-498.

Kwon, Y., 2004, Finite element analysis of planar 4:1 contraction flow with the tensor-logarithmic formulation of differential constitutive equations, *Korea-Australia Rheology J.* **16**, 183-191.

Leonov, A.I., 1976, Nonequilibrium thermodynamics and rheology of viscoelastic polymer media, *Rheol. Acta* **15**, 85-98.

Yoon, S. and Y. Kwon, 2005, Finite element analysis of viscoelastic flows in a domain with geometric singularities, *Korea-Australia Rheology J.* **17**, 99-110.